Applied Physics Letters

Large imprint in epitaxial $0.67Pb(Mg_{1/3}Nb_{2/3})O_3$-$0.33PbTiO_3$ thin films for piezoelectric energy harvesting applications

Cite as: Appl. Phys. Lett. **121**, 182903 (2022); https://doi.org/10.1063/5.0115777
Submitted: 27 July 2022 • Accepted: 08 October 2022 • Published Online: 03 November 2022

J. Belhadi, Z. Hanani, U. Trstenjak, et al.

Applied Physics Letters ARTICLE scitation.org/journal/apl

Large imprint in epitaxial $0.67Pb(Mg_{1/3}Nb_{2/3})O_3$-$0.33PbTiO_3$ thin films for piezoelectric energy harvesting applications

Cite as: Appl. Phys. Lett. **121**, 182903 (2022); doi: 10.1063/5.0115777
Submitted: 27 July 2022 · Accepted: 8 October 2022 ·
Published Online: 3 November 2022

J. Belhadi,[1,2] Z. Hanani,[2] U. Trstenjak,[2] N. A. Shepelin,[3] V. Bobnar,[4] G. Koster,[2,5] J. Hlinka,[6] D. Pergolesi,[3] T. Lippert,[3] M. El Marssi,[1] and M. Spreitzer[2,a)]

AFFILIATIONS

[1]Laboratory of Physics of Condensed Mater (LPMC), University of Picardie Jules Verne, Amiens 80039, France
[2]Advanced Materials Department, Jožef Stefan Institute, Jamova cesta 39, 1000 Ljubljana, Slovenia
[3]Laboratory for Multiscale Materials Experiments, Paul Scherrer Institute, Forschungsstrasse 111, 5232 Villigen PSI, Switzerland
[4]Condensed Matter Physics Department, Jožef Stefan Institute, Jamova 39, 1000 Ljubljana, Slovenia
[5]MESA+ Institute for Nanotechnology, University of Twente, 7500 AE Enschede, The Netherlands
[6]Department of Dielectrics, Institute of Physics of the Czech Academy of Sciences, Na Slovance 2, 182 21 Prague 8, Czech Republic

Note: This paper is part of the APL Special Collection on Piezoelectric Thin Films for MEMS.
[a)]**Author to whom correspondence should be addressed:** matjaz.spreitzer@ijs.si

ABSTRACT

Tuning and stabilizing a large imprint in epitaxial relaxor ferroelectric thin films is one of the key factors for designing micro-electromechanical devices with an enhanced figure of merit (FOM). In this work, epitaxial 500 nm-thick $0.67Pb(Mg_{1/3}Nb_{2/3})O_3$–$0.33PbTiO_3$ (PMN–33PT) films, free from secondary phases and with extremely low rocking curves (FWHM $< 0.05°$), are grown on $ScSmO_3$ (SSO) and $DyScO_3$ (DSO) substrates buffered with $SrRuO_3$ (SRO). The PMN–33PT is observed to grow coherently on SSO substrates (lattice mismatch of −0.7%), which is *c*-axis oriented and exhibits large tetragonality compared to bulk PMN–33PT, while on DSO substrates (lattice mismatch of −1.9%), the PMN–33PT film is almost completely relaxed and shows reduced tetragonality. Due to the compressive epitaxial strain, the fully strained PMN–33PT film displays typical ferroelectric P–E hysteresis loops, while the relaxed sample shows relaxor-like P–E loops. Samples present large negative imprints of about −88.50 and −49.25 kV/cm for PMN–33PT/SRO/SSO and PMN–33PT/SRO/DSO, respectively, which is more than threefold higher than the coercive field. The imprint is induced by the alignment of defect dipoles with the polarization and is tuned by the epitaxial strain. It permits the stabilization of a robust positive polarization state ($P_r \sim 20\,\mu C/cm^2$) and low dielectric permittivity (<700). In addition, the relaxed PMN–33PT film shows improved piezoelectric properties, with a 33% enhancement in $d_{33,eff}$ relative to the fully strained sample. The obtained low dielectric permittivity and the high piezoelectric coefficients at zero electric field in the studied PMN–33PT films hold great promise to maximize the FOM toward applications in piezoelectric devices.

Relaxor ferroelectrics are regarded as suitable candidates for active sensing, transduction, and piezoelectric energy harvesting applications, due to their excellent piezoelectric properties.[1,2] Generally, this enhancement is attributed to the coexistence of polar nanoregions (PNRs) and nanoscale inhomogeneities. Among these materials, $(1-x)Pb(Mg_{1/3}Nb_{2/3})O_3$–$xPbTiO_3$ (PMN–PT) solid solutions possess remarkable piezoelectric properties (piezoelectric coefficient, $d_{33} > 1500$ pC/N, and electromechanical coupling factor, $k_{33} > 0.9$) near the morphotropic phase boundary (MPB).[3–5] These properties can be achieved exclusively in PMN–PT single crystalline form with (001) orientation.[6]

In thin films, the substrate and the growth mode have a huge effect on the structural characteristics and functional properties of the PMN–PT material.[7–10] For instance, the piezoelectric coefficients in thin films are an order of magnitude lower relative to bulk PMN–PT single crystals due to substrate clamping.[10] PMN–PT thin films demonstrate slimmer ferroelectric polarization–electric field (P–E) hysteresis loops with low remanent polarization compared to the bulk material, which is beneficial, for instance, for energy storage applications. However, the low remanent polarization limits the application of PMN–PT in piezoelectric energy harvesting applications working at

zero electric field. Noting also, due to the high volatility of lead and the compositional complexity of PMN–PT, the synthesis of high-quality thick films (thickness > 500 nm) free from non-piezoelectric pyrochlore phases is challenging. Thus, controlling the growth of high quality and pure PMN–PT thin films and developing strategies for enhancing the piezoelectric properties are necessary for the development of high-performance energy harvesting devices.

An important strategy for the improvement of the piezoelectric response in thin films is the tailoring of imprint behavior of the *P–E* hysteresis loops.[11] The internal electric field in the films stabilizes one favorable polarization state at zero field, resulting in reduced aging in the piezoelectric devices and improved resistance to voltage- or temperature-dependent depolarization.[12] Moreover, the built-in potential suppresses the permittivity at zero field with minimal impact on the magnitude of the polarization. Accordingly, the figure of merit (FOM) for piezoelectric energy harvesting is increased, $FOM = \frac{e_{31f}^2}{\varepsilon_{33}\varepsilon_0}$ (e_{31f}, ε_{33}, and ε_0 are the transverse piezoelectric coefficient, relative dielectric permittivity, and dielectric permittivity in vacuum, respectively).[11]

Baek *et al.* have reported the energy harvesting properties of PMN–PT epitaxial thin film grown on $SrRuO_3/SrTiO_3/Si$ wafers, correlating the large FOM to a high e_{31f} value and a relatively low ε_{33} at zero-field.[13] Nevertheless, the stated zero-field relative dielectric permittivity reported by the authors is still too large (≈1500) to benefit from the imprint behavior.

In this Letter, high quality, pure, (001)-oriented, and epitaxial $67Pb(Mg_{1/3}Nb_{2/3})O_3$–$33PbTiO_3$ (PMN–33PT) thin films with $SrRuO_3$ (SRO) bottom electrode were grown by pulsed-laser deposition (PLD) on ScO_2-terminated (011)-oriented $DyScO_3$ (DSO) and $SmScO_3$ (SSO) substrates. The PMN–33PT films with a thickness of ∼500 nm were prepared from a ceramic target with 20 mol. %PbO and 20 mol. % MgO excess. Details about the PLD growth conditions of SRO and PMN–33PT can be found elsewhere.[7] The used SSO and DSO substrates provide different lattice mismatch with PMN-33PT, which could be calculated using the relation $\boldsymbol{f} = (\boldsymbol{a_s} - \boldsymbol{a_f})/\boldsymbol{a_s}$, where $\boldsymbol{a}_s$ and $\boldsymbol{a_f}$ are the lattice parameters of the substrate and the unstrained film, respectively. The obtained lattice mismatch is relatively small for PMN-33PT/SSO ($\boldsymbol{f} \sim -0.7\%$), while for PMN-33PT/DSO, it is quite large ($\boldsymbol{f} \sim -1.9\%$). In order to reduce the strain energy, applied epitaxial compressive strain relaxes above the critical thickness. Such relaxation is proportional to the lattice mismatch and is, thus, limited for the PMN-33PT/SSO system and more pronounced in the PMN-33PT/DSO case, providing two 500 nm-thick PMN-33PT examples with different strain states. *In situ* reflection high-energy electron diffraction (RHEED) (STAIB Instruments) was used to monitor the surface quality of SRO and PMN–33PT layers. High-resolution x-ray diffraction (HR-XRD), θ–2θ scans, rocking curves (RCs), and reciprocal-space maps (RSMs) were performed using high-resolution x-ray diffractometer (Empyrean, Malvern PANalytical) to analyze the purity, the strain state, and the epitaxial crystalline quality of the films. The *P–E* loops and the capacitance-electric field (*C–E*) curves of the samples were measured in parallel plate capacitor geometry with sputtered Au top-electrodes using an aixACCTTF-3000 analyzer system. The dielectric measurements as a function of the frequency were performed using an LCR meter (Agilent 4284) with probing ac amplitude of 100 mV. The piezoelectric properties of the PMN–33PT capacitors were determined using a double-beam laser interferometer (aixACCT aixDBLI).

The θ–2θ XRD scans around the (001) and (002) reflection peaks of the PMN–33PT/SRO heterostructures grown on DSO and SSO substrates are shown in Fig. 1(a). The full θ–2θ XRD scans of the films are shown in the supplementary material Fig. S1. The figures reveal that the PMN–33PT films are epitaxial, (00*l*) oriented, single-phase, and pyrochlore-free. Only a minor amount of (011) orientation (<0.05%) can be seen on the logarithmic scale for the film grown on SSO. The presence of Laue fringes around the main diffraction peaks of SRO (Fig. 1) is indicative of the high quality and epitaxial PMN–33PT/SRO heterostructures.[7]

The rocking curves obtained on the (002) peak of SRO and PMN–33PT layers [Fig. 1(b)] reveal narrow full width-at-half maximum (FWHM) values of $0.04^\circ < \Delta\omega < 0.06^\circ$, indicating very low mosaicity and confirming the excellent crystalline quality of the PMN–33PT/SRO heterostructures. The quality of PMN–33PT thin films is further confirmed by RHEED, revealing smooth surfaces [see Fig. S2(b) in the supplementary material]. Interestingly, despite the increased thickness of the studied PMN–33PT films (∼500 nm), the obtained $\Delta\omega$ values are as low as the values obtained, in general, on fully strained epitaxial thin films with a thickness of <100 nm.[7,14]

Such quality of the PMN–33PT films is achieved by using coherent and smooth SRO buffer layer grown on high quality single terminated substrates [see Fig. S2(a) in the supplementary material] and by carefully adjusting the PLD growth parameters. It is worth mentioning that, in general, the lack of high-quality epitaxial films, due to the thickness-dependent strain relaxation and the formation of undesired pyrochlore phases in thick PMN–PT films, has hindered the study of the effect of epitaxial strain on the structural characteristics and the functional properties.

Figure 1(a) shows that the 2θ position of the PMN–33PT diffraction peaks varies between the two samples grown on DSO and SSO, although both are shifted to lower angles compared to the bulk material, revealing that the films are under a compressive strain with different out-of-plane lattice parameters (*c*-axis). In order to access the in-plane lattice parameters (*a*-axis) and the strain state of each film, we further analyzed the structure by RSMs around the (0 -13) asymmetric reflection. The RSMs of the studied samples are shown in Fig. 1(c), and the obtained lattice parameters and the tetragonality (*c*/*a*) are gathered in Table I.

Figure 1(c) shows that the SRO layer is fully strained to the substrate in both samples, while the PMN–33PT layer is fully strained on the SSO substrate (SSO provides a relatively low lattice mismatch of −0.7% with PMN–33PT) and partially relaxed on DSO substrate (DSO provides a high lattice mismatch of −1.9% with PMN–33PT). In the fully strained PMN–33PT film, the biaxial strain induced a large tetragonal distortion with a large c-axis and high tetragonality ($c/a = 1.021$). The obtained tetragonality is close to that of the ferroelectric PMN–40PT composition in bulk material.[8] However, for the sample grown on the DSO substrate, the epitaxial strain of the PMN–33PT film is relaxed as a function of the thickness. In this case, the film demonstrates a low tetragonality enhancement ($c/a = 1.004$) with respect to the bulk. The obtained results show the possibility to engineer the strain state of the material through smooth templates with varying lattice mismatch, even in relatively thick films. Obtained θ–2θ scans and RSMs indicate that the lattice parameters are not homogeneous in the PMN-33PT films. Such variations could arise from a strain gradient due to gradual relaxation of the epitaxial strain and/or a change in the

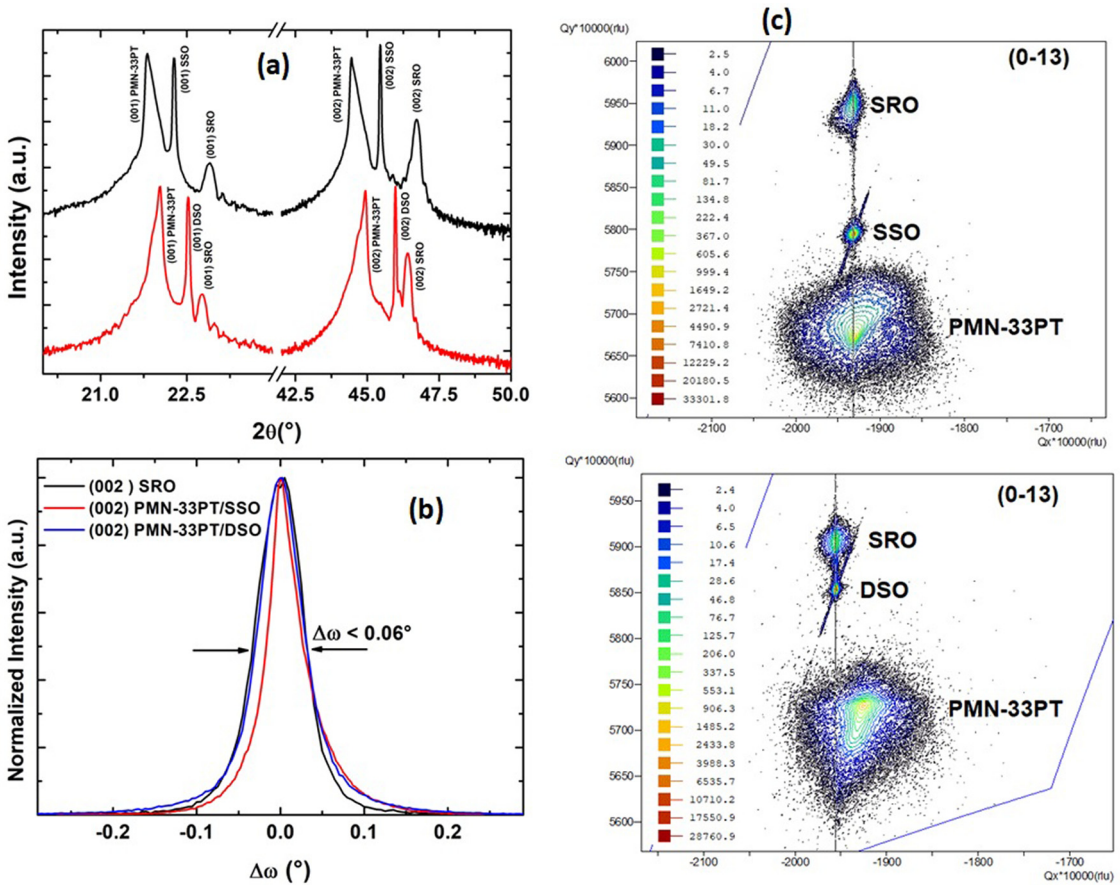

FIG. 1. (a) Magnified θ–2θ XRD patterns around the (001) and (002) reflections for PMN–33PT/SRO heterostructures grown on DSO and SSO substrates, (b) rocking curves around the (002) reflection of SRO and PMN–33PT layers, and (c) asymmetrical RSMs of the two studied PMN–33PT/SRO heterostructures.

TABLE I. Comparison of lattice parameters, remanent and maximum polarization, coercive field, imprint, and piezoelectric coefficient of PMN–33PT/SRO heterostructures grown on SSO and DSO substrate.

Substrate	c (Å)	a (Å)	c/a	$P_s(\mu C/cm^2)$	$P_{r+}(\mu C/cm^2)$	E_c(kV/cm)	E_s(kV/cm)	$d_{33,eff}$ (pm/V) at $E=0$
SSO	4.073	3.990	1.021	37.5	22	−39.73	−88.50	40
DSO	4.032	4.017	1.004	40.5	19	−14.73	−49.25	60

chemical composition (stoichiometry gradient) throughout the thickness of the film.

In order to evaluate the effect of strain-induced structural changes in PMN–33PT films on the functional properties, we measured their ferroelectric, dielectric, and piezoelectric responses. Figures 2(a) and 2(b) show the ferroelectric hysteresis loops and the dielectric permittivity (calculated from C–E curves) as a function of the applied electric field for the two PMN–33PT/SRO heterostructures, respectively.

First, the P–E loop of the PMN–33PT/SRO/SSO with enhanced tetragonality displays a typical ferroelectric behavior with a spontaneous polarization (P_s) of 37.5 μC/cm^2 and a remanent polarization (P_{r+}) of 22 μC/cm^2 for an applied electric field of 300 kV/cm. However, the shape of the P–E loop of PMN–33PT/SRO/DSO becomes slimmer with $P_s = 40.5$ and $P_{r+} = 19\,\mu$C/cm^2 at the same electric field. The relaxor-like behavior of this sample is attributed to the reduction of the tetragonality compared to the sample grown on SSO.

Second, the P–E loops of both PMN–33PT films show a very large negative electric-field shift (E_s, alternatively called imprint, self-bias field or internal built-in field throughout literature) for a positive voltage applied on the Au top electrode. This means that the E_s is directed from the top electrode to the bottom electrode in parallel with the applied electric field. The obtained $E_s = (E_{c+} + E_{c-})/2)$ was found to be of −49.25 and −88.50 kV/cm for the samples grown on DSO and SSO, respectively. This large E_s in Au/PMN–33PT/SRO capacitors is also observed in the ε_r–E curves, as shown in Fig. 2(b). Accordingly,

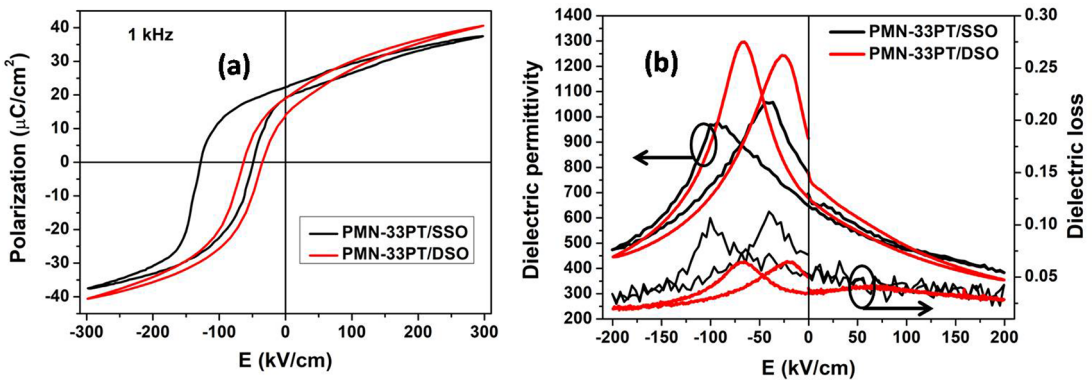

FIG. 2. (a) Polarization hysteresis loops and (b) dielectric permittivity and losses as a function of DC bias of PMN–33PT/SRO heterostructures grown on DSO and SSO substrates.

the large imprint results in a drastic decrease in the dielectric permittivity at zero electric field [$\varepsilon_r(E=0)$]. The value of $\varepsilon_r(E=0)$ is equal to approximately half of $\varepsilon_r(E_c)$, which is critical, for example, for the enhancement in the FOM of piezoelectric energy harvesting systems operating in the absence of external fields. In addition, the large E_s results in minimal dielectric losses at $E=0$ ($\mathrm{tg}\delta < 5\%$ at 1 kHz in the studied samples). The E_s, E_c, P_m, and P_r of PMN–33PT films are shown in Table I.

From Table I, a close relationship is observed between the strain state and tetragonality, and the imprint and coercive field of the PMN–33PT capacitors. Furthermore, it is evident that, in the PMN–33PT/SRO/SSO sample, a substrate-induced in-plane compressive strain (high c/a) stabilizes a tetragonal structure with the polarization oriented along the c-axis resulting in a well-saturated ferroelectric hysteresis loop with high E_c (in this case, the polarization reversal requires larger electric fields). However, in the PMN–33PT/SRO/DSO, we assume that the initial rhombohedral-like structure of the bulk is less distorted due to strain relaxation, giving rise to a slimmer and relaxor-like hysteresis loop with lower E_c. Noting that the built-in bias is larger than the coercive field in both films (E_s is twofold and threefold higher than E_c for the films grown on SSO and DSO, respectively), which results in breaking of the ferroelectric polarization degeneracy and the stabilization of a preferential polarization state (i.e., robust self-poling).

Despite the multitude of reports on the imprint in lead-based thin films,[13,15–18] determining the origin of this phenomenon is not straightforward due to the contribution of many extrinsic and intrinsic factors. Such factors comprise defect dipoles, trapped carriers, oxygen vacancies, strain gradients, and asymmetric electrodes, among others. For instance, a large negative imprint was reported by Baek *et al.* in the SRO/PMN–33PT/Pt capacitor, which has been attributed to the asymmetry between the top and bottom electrodes.[13] Moreover, Nguyen *et al.* have argued that a self-bias (56.2 kV/cm) in 300 nm-thick $Pb(Zr_{0.52}Ti_{0.48})_{0.99}Nb_{0.01}O_3$ (PNZT) capacitors with symmetric electrodes is caused by the accumulation of charges at the interface between the bottom electrode and PNZT film.[11] The authors suggest the mechanism to be defect incorporation driven by Nb-doping during the growth, causing strain gradients near the interface. The strain gradient at interfacial layers of $PbZr_{1-x}Ti_xO_3$ (PZT) has also been employed to tune the self-bias field in 200 nm-thick epitaxial PMN–33PT thin films sandwiched between symmetric SRO electrodes.[15] In compositionally graded 50–150 nm thick PZT films, Agar *et al.* have reported a complex evolution of built-in potential, which was found to be dependent on the combination of a strain gradient (via flexoelectric effect), a chemical gradient, and local inhomogeneities.[19] Recently, Kim *et al.* have reported a large positive self-bias in ion-bombarded 150 nm thick PMN–32PT capacitors with top and bottom SRO electrodes and attributed this imprint to the formation of intrinsic complex polar defects created by the high-energy ion bombardment.[20]

In the present study, given the relatively high thickness of the PMN–33PT layer (500 nm) in our capacitors, we assume that the very large observed imprint cannot be explained only by the asymmetry effect of the electrodes. As is the case in ion-bombarded PMN–PT films, we argue that the imprint in our capacitors is due to the formation of defect dipoles during the growth (to maintain the overall electrical charge neutrality of the sample) and their coupling with the strain/polarization. The obtained difference in the imprint between the two PMN-33PT films could be explained by the strain state/tetragonality of each of the samples. The formation of defect dipoles complexes between, for instance, the oxygen and either lead, magnesium, or titanium vacancies, leads to very low dielectric losses in a wide frequency range from 10 Hz to 100 kHz (see Fig. S3 in the supplementary material), as demonstrated by low leakage current in ion-bombarded PMN-33PT thin films with polar defects.[20] Such films permit the stabilization of the ferroelectric state against temperature fluctuations. Noting that the presence of the strain gradient in a portion of the PMN-33PT films is likely contributing to the imprint by aligning the defect dipoles. Notably, the possible effects of local chemical gradients and inhomogeneities on the imprint cannot be excluded in our films and, thus, call for further investigation.

Stabilizing such large self-bias in as-grown epitaxial relaxor ferroelectric thin films and controlling its magnitude via strain engineering are of high importance and could be considered as powerful routes to design materials with high piezoelectric energy harvesting performances without using additional buffer interlayers, doping, or ex-situ treatments. Thus, we have investigated the piezoelectric performance of the PMN–33PT films, which is shown in Fig. 3.

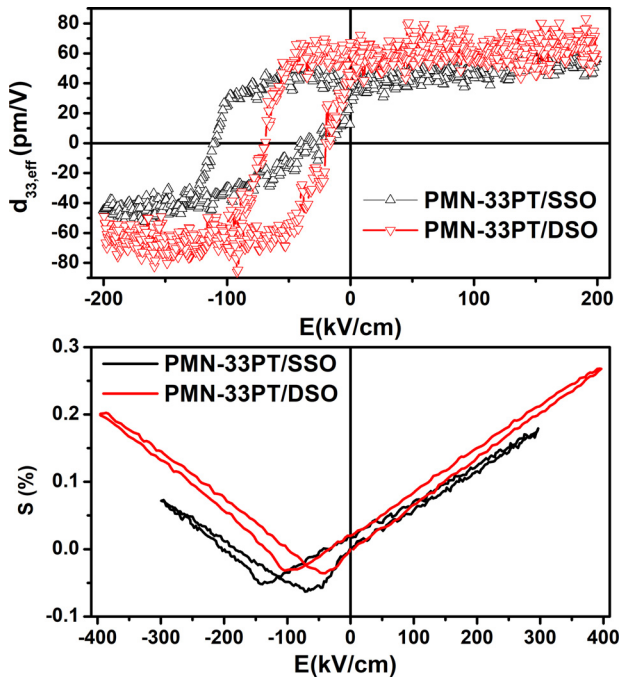

FIG. 3. (a) Longitudinal piezoelectric coefficient $d_{33,eff}$ and (b) large-signal piezoelectric strain response S of PMN–33PT/SRO heterostructures grown on DSO and SSO substrate.

As in the case of *P*–*E* loops and ε_r–*E* curves, a large imprint is also obtained in the measurements of the piezoelectric properties. The same trend of increasing imprint and coercive field with increasing the tetragonality of the films is also observed in the longitudinal piezoelectric coefficient [Fig. 3(a)] and the large-signal piezoelectric strain [Fig. 3(b)] measurements. Since $E_s > E_c$, a maximum self-piezoelectric response (at zero field) is obtained in both samples. The PMN–33PT film grown on DSO demonstrates an enhanced $d_{33,eff}$ and displacement compared to the strained film grown on SSO, which could be attributed to the stabilization of the relaxor state in the former and/or the decreased domain wall mobility (extrinsic contribution) in the latter. As is the case for most studies on thin films, the obtained $d_{33,eff}$ values are an order of magnitude lower than in bulk materials, due to the strong underlying substrate-clamping effect.

In summary, pure and high crystalline quality 500 nm-thickPMN–33PT films with extremely low rocking curve values were grown by PLD on SRO buffered SSO and DSO substrates. Under compressive epitaxial strain, high teragonality and ferroelectric-like P-E loops are stabilized in the PMN–33PT film grown on an SSO substrate (SSO provides a relatively small lattice mismatch with the PMN–33PT). However, for the PMN–33PT grown on substrate with a larger lattice mismatch, i.e., on DSO, the strain is relaxed, and the film displays a relaxor-like P–E loop and enhanced $d_{33,eff}$. Both the strained and relaxed SRO/PMN–33PT/Au capacitors exhibit a very large negative self-bias of about −88.50 and −49.25 kV/cm, respectively, which result in a low dielectric permittivity at E = 0. The permittivity values obtained in this study are the lowest reported in thick PMN–33PT films to date and are comparable to that obtained in PZT based thin films with the highest FOM. Since PMN–PT materials are known to possess improved piezoelectric properties compared to PZT, our findings demonstrate the possibility to further enhance the FOM of piezoelectric devices based on high quality PMN–PT thin films.

See the supplementary material for θ–2θ XRD full scans of the samples, RHEED patterns of SRO and PMN-33PT layer, and the dielectric permittivity and dielectric losses as a function of the frequency of Au/PMN-33PT/SRO/SSO.

This research was financially supported by the Slovenian Research Agency (Nos. P2-0091, J2-2510, N2-0187, N2-0149, and P1-0125), the Swiss National Science Foundation (Lead Agency Grant No. 192047), the Strategy AV21 framework of the Czech Academy of Sciences, programme Efficient Energy Conversion and Storage. J.B. and M.E. gratefully acknowledge the generous financial support of the Region Hauts-de-France (Project TERRA) and the European Union Horizon 2020 Research and Innovation actions MSCA-RISE-ENGIMA (No. 778072) and MSCA-RISE-MELON (No. 872631).

AUTHOR DECLARATIONS

Conflict of Interest

The authors have no conflicts to disclose.

Author Contributions

Jamal Belhadi: Conceptualization (equal); Formal analysis (equal); Investigation (equal); Methodology (equal); Writing – original draft (equal). **Mimoun EL Marssi:** Investigation (equal); Writing – review & editing (equal). **Matjaž Spreitzer:** Conceptualization (equal); Funding acquisition (equal); Investigation (equal); Supervision (equal); Writing – review & editing (equal). **Zouhair Hanani:** Investigation (equal); Writing – original draft (equal). **Urška Trstenjak:** Investigation (equal); Writing – review & editing (equal). **Nikita Shepelin:** Investigation (equal); Writing – review & editing (equal). **Vid Bobnar:** Investigation (equal); Writing – review & editing (equal). **Gertjan Koster:** Investigation (equal); Writing – review & editing (equal). **Jirka Hlinka:** Investigation (equal); Writing – review & editing (equal). **Daniele Pergolesi:** Investigation (equal); Writing – review & editing (equal). **Thomas Lippert:** Investigation (equal); Writing – review & editing (equal).

DATA AVAILABILITY

The data that support the findings of this study are available from the corresponding author upon reasonable request.

REFERENCES

[1]F. Li, S. Zhang, T. Yang, Z. Xu, N. Zhang, G. Liu, J. Wang, J. Wang, Z. Cheng, Z.-G. Ye, J. Luo, T. R. Shrout, and L.-Q. Chen, Nat. Commun. **7**, 13807 (2016).
[2]S. Zhang, F. Li, X. Jiang, J. Kim, J. Luo, and X. Geng, Prog. Mater. Sci. **68**, 1–66 (2015).
[3]F. Li, M. J. Cabral, B. Xu, Z. Cheng, E. C. Dickey, J. M. LeBeau, J. Wang, J. Luo, S. Taylor, W. Hackenberger, L. Bellaiche, Z. Xu, L.-Q. Chen, T. R. Shrout, and S. Zhang, Science **364**, 264 (2019).
[4]Q. Li, Y. Liu, J. Liu, K. Song, H. Guo, F. Li, and Z. Xu, Adv. Funct. Mater. **32**, 2201719 (2022).

[5]H. Katzke, M. Dietze, A. Lahmar, M. Es-Souni, N. Neumann, and S.-G. Lee, Phys. Rev. B **83**, 174115 (2011).
[6]S.-H. Baek, M. S. Rzchowski, and V. A. Aksyuk, MRS Bull. **37**, 1022 (2012).
[7]J. Belhadi, U. Gabor, H. Uršič, N. Daneu, J. Kim, Z. Tian, G. Koster, L. W. Martin, and M. Spreitzer, RSC Adv. **11**, 1222 (2021).
[8]U. Trstenjak, N. Daneu, I. Rafalovskyi, J. Belhadi, D. Vengust, J. Hlinka, and M. Spreitzer, Appl. Phys. Lett. **120**, 042901 (2022).
[9]R. Herdier, M. Detalle, D. Jenkins, C. Soyer, and D. Remiens, Sens. Actuators, A **148**, 122 (2008).
[10]J. H. Park and S. Trolier-McKinstry, J. Mater. Res. **16**, 268 (2001).
[11]M. D. Nguyen, E. Houwman, M. Dekkers, D. Schlom, and G. Rijnders, APL Mater. **5**, 074201 (2017).
[12]C. S. Han, K. S. Park, H. J. Choi, and Y. S. Cho, J. Alloys Compd. **720**, 369 (2017).
[13]S. H. Baek, J. Park, D. M. Kim, V. A. Aksyuk, R. R. Das, S. D. Bu, D. A. Felker, J. Lettieri, V. Vaithyanathan, S. S. N. Bharadwaja, N. Bassiri-Gharb, Y. B. Chen, H. P. Sun, C. M. Folkman, H. W. Jang, D. J. Kreft, S. K. Streiffer, R. Ramesh, X. Q. Pan, S. Trolier-McKinstry, D. G. Schlom, M. S. Rzchowski, R. H. Blick, and C. B. Eom, Science **334**, 958 (2011).
[14]J. Kim, H. Takenaka, Y. Qi, A. R. Damodaran, A. Fernandez, R. Gao, M. R. McCarter, S. Saremi, L. Chung, A. M. Rappe, and L. W. Martin, Adv. Mater. **31**, 1901060 (2019).
[15]M. Boota, E. P. Houwman, M. Dekkers, M. Nguyen, and G. Rijnders, Appl. Phys. Lett. **104**, 182909 (2014).
[16]J. Lee, R. Ramesh, V. G. Keramidas, W. L. Warren, G. E. Pike, and J. T. Evans, Appl. Phys. Lett. **66**, 1337 (1995).
[17]C. Lichtensteiger, C. Weymann, S. Fernandez-Pena, P. Paruch, and J.-M. Triscone, New J. Phys. **18**, 043030 (2016).
[18]C. Weymann, C. Lichtensteiger, S. Fernandez-Peña, A. B. Naden, L. R. Dedon, L. W. Martin, J.-M. Triscone, and P. Paruch, Adv. Electron. Mater. **6**, 2000852 (2020).
[19]J. C. Agar, A. R. Damodaran, G. A. Velarde, S. Pandya, R. V. K. Mangalam, and L. W. Martin, ACS Nano **9**, 7332 (2015).
[20]J. Kim, S. Saremi, M. Acharya, G. Velarde, E. Parsonnet, P. Donahue, A. Qualls, D. Garcia, and L. W. Martin, Science **369**, 81 (2020).